Title

Supramolecular meso-Trick: Ambidextrous Mirror Symmetry Breaking in a Liquid Crystalline Network with Tetragonal Symmetry

Journal

Journal of the American Chemical Society, 144(15)

ISSN

0002-7863

Authors

Cao, Yu

Alaasar, Mohamed

Zhang, Lei

et al.

Publication Date

2022-04-20

DOI

10.1021/jacs.2c01511

Supramolecular *meso*-Trick - Ambidextrous Mirror Symmetry Breaking in a Liquid Crystalline Network with Tetragonal Symmetry

Yu Cao,[1,2] Mohamed Alaasar,[3,4] Lei Zhang,[2] Chenhui Zhu,[5] Carsten Tschierske*[3] and Feng Liu*[1]

[1] Shaanxi International Research Center for Soft Matter, State Key Laboratory for Mechanical Behavior of Materials, Xi'an Jiaotong University, Xi'an 710049, P. R. China

[2] MOE Key Laboratory for Nonequilibrium Synthesis and Modulation of Condensed Matter, School of Physics, Xi'an Jiaotong University, Xi'an 710049, China

[3] Institute of Chemistry, Martin Luther University Halle-Wittenberg, Kurt Mothes Str. 2, D-06120 Halle (Saale), Germany

[4] Department of Chemistry, Cairo University, 12613 Giza, Egypt

[5] Advanced Light Source, Lawrence Berkeley National Laboratory, Berkeley, CA 94720, USA

Abstract: Bi- and multi-continuous network phases are among nature's most complex structures in soft matter systems. Here a chiral bicontinuous tetragonal phase is reported as a new stable liquid crystalline intermediate phase at the transition between two cubic phases, the achiral double gyroid and the chiral triple network cubic phase with *I*23 space group, both formed by dynamic networks of helices. The mirror symmetry of the double gyroid, representing a *meso*-structure of two enantiomorphic networks, is broken at the transition to this tetragonal phase by retaining uniform helicity only along one network while losing it along the other one. This leads to a conglomerate of enantiomorphic tetragonal space groups, $P4_12_12$ and $P4_32_12$. Phase structures and chirality were analyzed by small-angle X-ray scattering (SAXS), grazing-incidence small-angle X-ray scattering (GISAXS), resonant soft X-ray scattering (RSoXS) at the carbon K-edge and model-dependent SAXS/RSoXS simulation. Our findings not only lead to a new bicontinuous

network-type 3D mesophase but also reveals a mechanism of mirror symmetry breaking in soft matter by partial *meso*-structure racemization at the transition from enantiophilic to enantiophobic interhelical self-assembly.

1. Introduction

Complex nanostructured supermolecular systems build the basis of biological evolution as well as new materials.[1] Therefore, the fundamental understanding of the formation of such systems by simple molecules, especially the development of structural complexity[2-4] and emergence of chirality[5-14] are of importance. Emergence of chirality and amplification of asymmetry[15] by spontaneous helix formation were well investigated in the crystalline and solution aggregated states of chiral and achiral C_3 symmetric benzene-1,3,5-tricarboxamides[16-19] and related compounds.[6-9,20-25] However, for achiral molecules, at the transition to the liquid crystalline (LC) state supermolecular chirality is typically lost in the one-dimensional (1D) columnar assemblies due to emerging helix inversion defects.[20-23] Network formation by 3D branching the columns can remove these defects and synchronize the chirality in these network phases with cubic symmetry (bicontinuous cubic phases, Cub_{bi}), and even in some cases in the isotropic liquid mesophases occurring adjacent to them.[24-26] The Cub_{bi} phases have also attracted significant attention due to their structural complexity and importance in biological structures,[27-36] as well as for various applications, including ion transportation, catalysis, drug delivery, organic electronic devices and energy conversion.[33,37-41] The double network Cub_{bi} phase with $Ia\bar{3}d$ space group, known as double gyroid, and a second one with *I*23 space group and triple network structure (Figs. 1 and S1) are often observed for achiral rod-like π-conjugated molecules with at least two or more terminally attached flexible chains (polycatenar molecules).[42-46] The $Ia\bar{3}d$ phase is achiral, whereas the *I*23 phase was recently found to spontaneously form chiral conglomerates as observed by polarized optical microscopy (POM) and confirmed by circular dichroism (CD), thus indicating ambidextrous mirror symmetry breaking.[25,43-44,47-48] According to present knowledge, the chirality is a result of the organization of the rod-like molecules in short column segments, interconnected by three-way junctions with an orientation of the rods being on average

perpendicular to the local column directions. In this configuration, the clashing of the bulky alkyl chains leads to helicity of the molecular packing along these networks. The helix sense is synchronized along the individual networks by the junctions and obviously also communicated between the networks, leading to conglomerate formation. Such dynamic networks of self-assembled helical π-systems can assume uniform chirality under the directing influence of weak chirality sources or dopants due to their huge asymmetry amplification power.[26] Uniform chirality can also develop spontaneously in a stochastic way, if slow seed formation is coupled with fast growth of the chiral domain.[49] This is not only of potential technological interest for circular polarized emission[50] and other applications, but also offers a possible pathway of the development of homochirality in fluid systems[26,49], being of significance for the earliest stages of development of life.[49,51] On the other hand, the $Ia\bar{3}d$ phase of polycatenar molecules is achiral, though there is helicity along the networks, too (Fig. 1a).[25,52] In this case the chirality of the networks themselves and also the helix sense of the supramolecular helices in these networks are opposite and therefore cancel out, leading to an overall achiral *meso*-structure composed of two inseparably interwoven enantiomorphous networks. However, how mirror symmetry is broken at the transition from the achiral $Ia\bar{3}d$ to the chiral *I*23 phase (Fig. 1b) still remains unknown and their relationship is an open question. Revealing such relationship could not only be beneficial to the understanding of chirality generation during self-assembly in soft matter systems but also offer a new mode for self-assembly involving superstructural chirality.

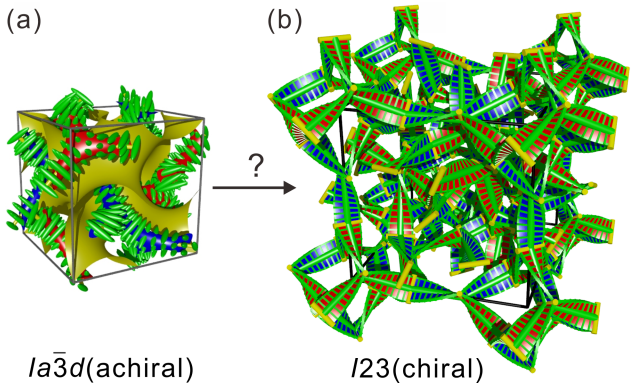

Fig. 1 (a) The achiral bicontinuous $Ia\bar{3}d$ phase contains two networks with opposite chirality[25]. Molecules along distinct networks (red & blue) have opposite sense of twist.

(b) The triple network model proposed for the ambidextrous chiral *I*23 phase.[47] Molecules along all networks share the same sense of twist; see Fig. S1 for alternative presentations; a) and b) were reproduced with permission from Refs. 25 and 47 with permission of Wiley-VCH (copyright 2014) and Royal Society of Chemistry (copyright 2020), respectively.

Here, a new chiral tetragonal LC phase (Tet_{bi}) is reported with chiral $P4_12_12/P4_32_12$ space group occurring as intermediate structure at the transition from the achiral $Ia\bar{3}d$ to the chiral *I*23 phase and a pathway of symmetry breaking at this transition is proposed. The cubic $Ia\bar{3}d$ and *I*23 phases themselves have been investigated previously[47,52] and are not subject of this work. A combination of small-angle X-ray scattering (SAXS), grazing-incidence small-angle X-ray scattering (GISAXS), resonant soft X-ray scattering (RSoXS) and model-dependent scattering simulation validates not only the morphology, but also the molecular packing in the enantiomorphic tetragonal LC phases with $P4_12_12/P4_32_12$ space groups. Based on these investigations, a model of the Cub_{bi}/$Ia\bar{3}d$-Tet_{bi} phase transition is proposed, involving racemization of every second helix of the double gyroid *meso*-structure of the $Ia\bar{3}d$ phase, due to a change of the dominating interhelical self-assembly from enantiophilic to enantiophobic.

2. Results

2.1 The material and its phase sequence

The material we studied is a polycatenar compound with a long anisotropic aromatic core containing five aromatic rings and in total four aliphatic tails distributed in a ratio 3:1 to both ends. Utilizing compound **1-18**, we systematically studied the phase behavior and raised the phase transition sequence shown in Fig. 2.

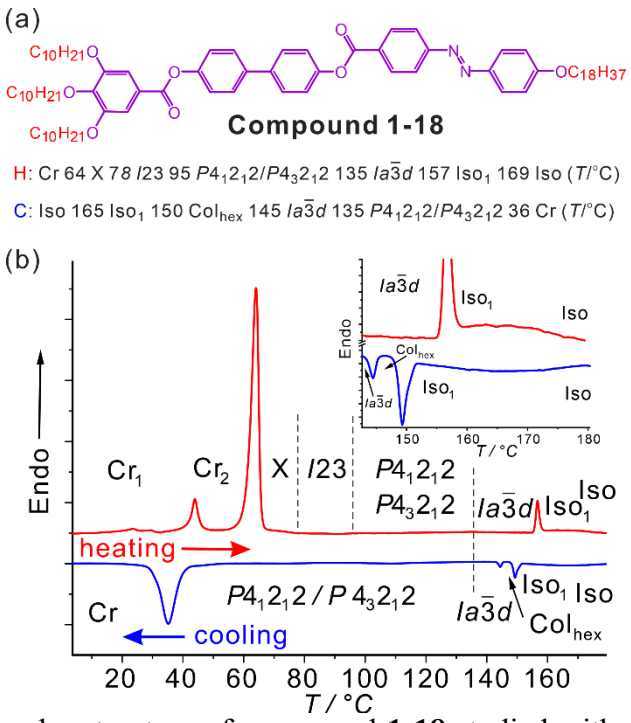

Fig. 2 (a) The molecular structure of compound **1-18** studied with phase sequence and transition temperatures; the Cr⟶X transition in the second heating is at 55 °C [23.0]; enthalpy values (kJ mol^{-1}) are listed in the brackets. (b) DSC curves (first heating and cooling, recorded at 10 K·min^{-1}. Abbreviations: Cr, Cr' = crystalline solids; Col_{hex} = hexagonal columnar LC phase; $Ia\bar{3}d$ and $I23$ are bicontinuous cubic LC phases (Cub_{bi}) with $Ia\bar{3}d$ and $I23$ space group, respectively; $P4_12_12/P4_32_12$ indicates a bicontinuous tetragonal LC phase (Tet_{bi}), representing a conglomerate of these two chiral space groups; Iso = isotropic liquid state and Iso_1 is a percolated isotropic liquid with local network structure; X is an unknown mesophase. $I23$ and $P4_12_12/P4_32_12$ are chiral, whereas the other phases are achiral.

The synthesis of compound **1-18** has been reported in a previous work which was focused on the confirmation of the helical superstructure in the $Ia\bar{3}d$ phase occurring between 135 and 157 °C on heating, whereas the other mesophases were not analysed in detail[52] and those are reported herein. Upon cooling from the isotropic liquid, at 150 °C, a typical spherulitic texture of a columnar phase is observed by polarizing optical microscopy (POM). Investigation with additional λ-plate, shows that this columnar phase is optically negative, i.e., the molecular long axis is supposed to be perpendicular or only slightly tilted to the columnar long axis (Fig. S2a, b). GISAXS confirms the columnar phase and indicates a hexagonal lattice (Col_{hex}), see Fig. S3 and Table S1. The lattice parameter a_{hex} = 5.07 nm in this columnar phase is 0.77 × L_{mol} (L_{mol} = molecular lengths = 6.6 nm in the most stretched conformation) which is in the typical range considering the chain folding

around the columns. In this columnar phase the molecules are organized in strata of about 5 molecules which pack on top of each other, thus forming the column cores embedded in the continuum of the alkyl chains. The texture becomes completely dark upon cooling to 145 °C as the cubic $Ia\bar{3}d$ phase is generated. At this transition the columns involving the π-conjugated rods become branched and the resulting interpenetrated networks are separated by the gyroid infinite periodic minimal surfaces located in the aliphatic continuum, half way between the networks. A relatively weak birefringence returns below 135 °C as a sign of a transition to a non-cubic mesophase. No significant change, except for a slight continuous increase of birefringence, can be observed upon further cooling down to 40 °C when the sample crystallizes (Fig. S2c, d). Upon heating, the crystals melt at 64 °C and the birefringence decreases slowly in the temperature range of the X-phase until the texture becomes optically isotropic at 78 °C, indicating the transition to another Cub_{bi} phase which was identified as *I*23 phase by SAXS (see Fig. 3c,f and discussions further below). Upon further heating, a weak birefringence occurs again at 95 °C and disappears at 135 °C at the transition to the $Ia\bar{3}d$ phase which at 157 °C transforms without intermediate formation of a Col_{hex} phase to the isotropic liquid, i.e. the columnar phase is only metastable. Though it takes time to recrystallize upon cooling and different crystalline modifications can form, the heating and cooling cycles are reproducible for the LC phases of the same sample, verified by POM observations and SAXS patterns. This also indicates that the compound is (thermal and photochemical) stable under the experimental conditions. Serving as metastable phases, the formation of the X and adjacent Cub_{bi}/*I*23 phase relies on the conditions and the environment. Based on SAXS temperature scans, the X phase can be proved coexisting with the crystalline and continuously transferring between 78 and 95 °C to the Cub_{bi}/*I*23 phase which above this temperature range becomes birefringent (see Fig. S4). In DSC only melting, crystallization, the Cub_{bi}-Iso transitions and transitions involving the Col_{hex} phase are associated with sharp transition peaks, whereas the other phase transitions in the LC range are not visible (see Fig. 2). This might be because these transitions are continuous or slow. There is an additional broad feature in the isotropic liquid state (see inset in Fig. 2b, ΔH

~2.7 kJ mol^{-1}) which indicates a transition between an ordinary liquid (Iso) and an achiral percolated liquid with local network structure (Iso_1).[53-55] The wide-angle X-ray scattering (WAXS) has only one diffuse maximum around d = 0.42-0.43 nm in all mesophases occurring between the crystalline and the isotropic liquid state (the insets of Fig. 3a-c), i.e. these are liquid crystalline phases without fixed positions of the individual molecules.

2.2 The tetragonal phase - a stretched double gyroid network with chiral space group

SAXS was applied to probe the phase transitions, to identify the space groups (for SAXS data and indexation of the Cub_{bi} phases, see Tables S2 and S4), and to solve the unknown birefringent mesophase between the two Cub_{bi} phases, $I23$ and $Ia\bar{3}d$. Temperature scans of heating and cooling in steps of 5 °C suggested that the phase transition between the $I23$ phase and the birefringent mesophase is discontinuous while the transition to $Ia\bar{3}d$ is continuous (Fig. S5, S8a). Being an intermediate phase between the $I23$ and $Ia\bar{3}d$ phase, both involving continuous networks, the birefringent mesophase should have one of the Sohncke space groups with non-cubic symmetry. Taking the crystallographic group theory as a facile method, the symmetry of the birefringent mesophase is supposed to share the same super group with $I23$ and also serve as a subgroup of $Ia\bar{3}d$.[56] This suggests that the symmetry could potentially be one with 422 point group, which involves $I4_122$, a SmQ phase discovered before.[57] Fortunately, we found that the scattering signals merged as the Tet_{bi} phase turned into the $Ia\bar{3}d$ Cub_{bi} phase (Fig. S5a). Similarly, the signals split at the $Ia\bar{3}d$ → Tet_{bi} transition during cooling, as shown in Fig. S5b. This allows us to index the SAXS pattern of the Tet_{bi} phase in a similar way as $Ia\bar{3}d$, considering the deviation of lattice parameter. Such indexation is further supported by GISAXS patterns of orientated thin films. The scattering patterns match nicely with simulations containing two film orientations, see Fig. S7. The allowed space group with the highest symmetry is $P4_32_12$ and $P4_12_12$, a pair of chiral space groups with opposite chirality, see details in Table S3. Following such indexation, we obtained the lattice parameter and lattice volume of all three phases and their development depending on temperature (Fig. S8). By comparison between heating and cooling routines, we found

that the phase transition between the tetragonal and $Ia\bar{3}d$ phase is reversible and reproducible.

To reconstruct the electron density (ED) map of the tetragonal phase, the phase problem is first to be solved. $P4_12_12$ is a non-centrosymmetric space group, whose phase angle is not restricted to 0 or π as in the $Ia\bar{3}d$ Cub_{bi} phase. The continuous transition between the Tet_{bi} and $Ia\bar{3}d$ phase indicates the structural similarity of the two phases. To determine the phase angle of the $P4_12_12$ tetragonal phase, we raised a model by distorting the bicontinuous network of the $Ia\bar{3}d$ phase. The $Ia\bar{3}d$ phase is well known to contain two continuous networks separated by a Gyroid (G) minimal surface. Accordingly, we assumed that the $P4_12_12$ phase is a distorted $Ia\bar{3}d$ phase, which is separated by a distorted G minimal surface stretched along the *c* axis. Mathematically, the G minimal surface can be represented by the following equation.

$$\sin X \cos Y + \sin Z \cos X + \sin Y \cos Z = c; c = 0 \qquad (1)$$

The two networks are constructed by subsurfaces of the G minimal surface, i.e. $|c| > 0$. Here, we applied a pure mathematical model to estimate the phase angle of the tetragonal phase. First, bicontinuous networks were constructed based on the symmetry requirement of the $Ia\bar{3}d$ and $P4_12_12$ space groups as shown in Fig. 4a and 4c. The coordinates of junctions are listed in Table 1, in which we could derive that the networks of the $Ia\bar{3}d$ phase was shifted by *a*/4 and 3*c*/8 to obtain ones of $P4_12_12$ phase. Moreover, the extension of the constructed networks could reveal the fact that the $P4_12_12$ phase is actually an $Ia\bar{3}d$ phase elongated along the *c* axis.

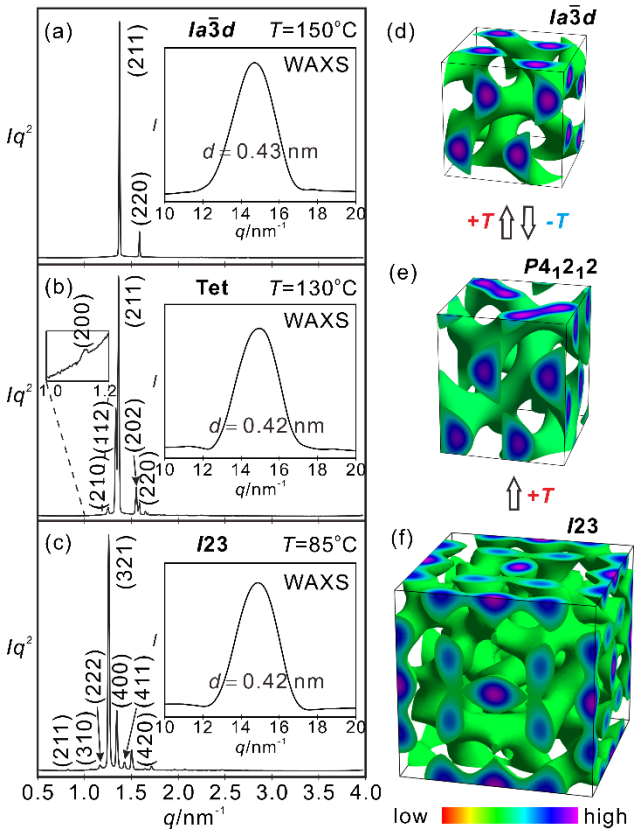

Fig. 3 (a-c) The SAXS diffractograms, lattice parameters and (d-f) reconstructed electron density (ED) maps of (a, d) $Ia\bar{3}d$ Cub_{bi} phase at 150 °C; (b, e) $P4_12_12/P4_32_12$ tetragonal phase at 135 °C and (c, f) $I23$ Cub_{bi} phase at 85 °C obtained by the phase combination reported before[47], for more details, see Fig. S6 and Tables S2-S4. The insets in (a-c) are the WAXS curves. High electron density is in purple, green are surfaces with intermediate density, low electron density regions in red are omitted for clarity, the complete electron density maps are shown in Fig. S9.

Table 1 Coordinates of the junctions of the $Ia\bar{3}d$ and $P4_12_12$ phases.

$Ia\bar{3}d$	red	(1,1,1)/8	(1,7,3)/8	(3,7,5)/8	(5,5,5)/8	(5,3,7)/8	(3,1,7)/8	(7,5,3)/8	(7,3,1)/8
	blue	(7,7,7)/8	(1,5,7)/8	(1,3,5)/8	(3,3,3)/8	(3,5,1)/8	(5,1,3)/8	(5,7,1)/8	(7,1,5)/8
$P4_12_12$	red	(3,1,4)/8	(3,7,6)/8	(5,7,8)/8	(7,5,8)/8	(7,3,2)/8	(5,1,2)/8	(1,5,6)/8	(1,3,4)/8
	blue	(1,7,2)/8	(3,5,2)/8	(3,3,8)/8	(5,3,6)/8	(5,5,4)/8	(7,1,6)/8	(7,7,4)/8	(1,1,8)/8

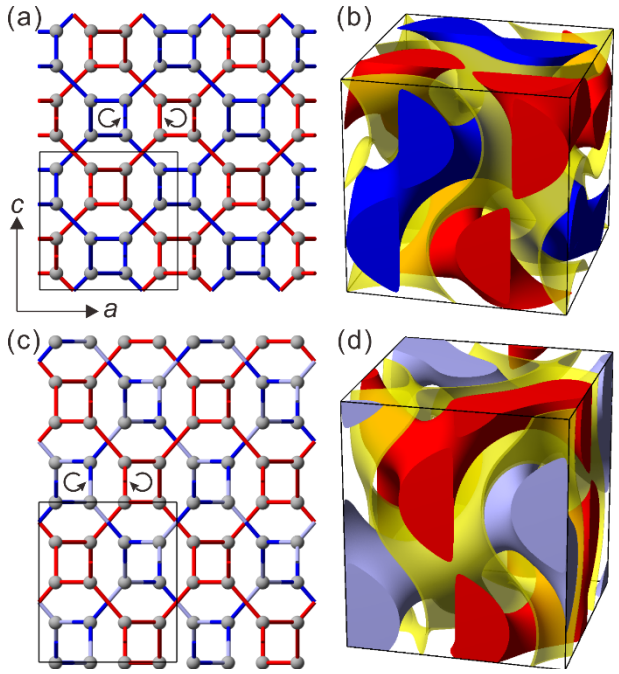

Fig. 4 (a, c) Bicontinuous networks in space group of $Ia\bar{3}d$ and $P4_12_12$ respectively; gray spheres, indicating the junctions, are located at the coordinates in Table 1. Networks with distinct color represent opposite chirality. The $P4_12_12$ phase is an elongation of the $Ia\bar{3}d$ phase along *c* direction after shifting *a*/4 and 3*c*/8. Unlike the achiral $Ia\bar{3}d$ phase, the blue network is different from the red network, which breaks the symmetry and makes $P4_12_12$ a chiral phase; (b, d) G minimal surface (in yellow), separating two interwoven networks and subsurfaces enclosing the aromatic regions (in the same color as the networks in a, c), is constructed by Equation 1 for both phases.

Second, based on the elongation and shift of the junctions, a distorted G minimal surface was constructed for the $P4_12_12$ space group (yellow in Fig. 4d). Third, a series of subsurfaces was constructed to form the distorted bicontinuous network. A higher constant value was set for the volume enclosed by the networks and, in contrast, lower constant is elsewhere. By assuming $|c| = 1.01$, we obtained mathematical models of both phases, $Ia\bar{3}d$ and $P4_12_12$, whose volume ratio between networks and lattice (33.4%) are similar to the aromatic ratio in the single molecule (36.5%, see Table S5), i.e. the subsurface is the boundary between the aromatic/aliphatic region, as shown in Fig. 4b, d. Finally, we conducted Fourier transform to the mathematical models to compute the phase angles and simulated scattering intensity of the four strongest signals (112), (211), (202) and (220), see details in Section 4 of the SI, Fig. S11 and Table S6. The phase angle of (112) is π, which is in line with symmetry requirement as (*hhl*) should be either 0 or π

when *l* is even. The ED maps of all three phases were reconstructed and are shown in Fig. 3. Moreover, the d*V*/d*r* curves were computed based on the constructed networks and minimal surfaces for *I*23, Tet_{bi}, $Ia\bar{3}d$ and Col_{hex} phases. Both peak and tail of the curves suggest a phase transition sequence of *I*23-Tet_{bi}-$Ia\bar{3}d$-Col_{hex} upon heating, which is in line with experimental observation, see details in Fig. S13 and accompanied explanations in Section 5 of the SI.

2.3 Deciphering the helical nature of the tetragonal phase by resonant soft X-ray scattering

The enantiomorphic space groups $P4_12_12$/$P4_32_12$ suggests that chirality is generated upon phase transition from $Ia\bar{3}d$ to Tet_{bi}, but what breaks the symmetry of the $Ia\bar{3}d$ phase in the Tet_{bi} phase and how to further prove the validity of the enantiomorphic space groups determined by SAXS? Due to the linear birefringence of the Tet_{bi} phase, which is much larger than the optical effects due to rotation of the plane of the polarized light, chiroptical methods cannot be applied in this case. To solve this problem and to answer these questions, we utilized RSoXS, representing a powerful tool probing molecular orientational order and helical self-assembly[58] in birefringent systems[52,59-68] with element sensitivity[69]. The temperature scan upon heating was recorded (Tables S7-S8); the phase transition between *I*23 and Tet_{bi} and the tetragonal lattice parameter variation are all in line with the non-resonant SAXS data and all signals can be properly indexed in all three phases. Normally, the 'forbidden peaks', which are not allowed by symmetry and absent in conventional SAXS, help in space group determination. In our system, the *I*23 phase didn't show any 'forbidden peak' but all observed signals are allowed by symmetry and resonant enhanced as shown in Fig. S14. The resonant enhancement is from the orientational order, i.e. the presence of uniform helicity along the networks of the *I*23 phase. Without this helicity, the intensity of the scattering signal is supposed to decrease due to absorption. The $Ia\bar{3}d$ phase exhibits the 'forbidden peaks' (110) and (200), as deciphered elsewhere.[52] Interestingly, several peaks can be observed in the Tet_{bi} phase, including two 'forbidden peaks' (100), (002) and several resonant enhanced peaks, the

2D image of a thick film at 120 °C is shown in Fig. 5(a) and a comparison between RSoXS and SAXS curves is shown in Fig. 5d-e. The black solid arcs cover 55 pixels, which indicates an error bar of maximum 0.5 nm, small enough for low-Miller indices in the figure to be reliable. The small deviation of the lattice parameters between RSoXS and SAXS could result from distinct thermal environment and sample states in the vacuum chamber of RSoXS investigations.

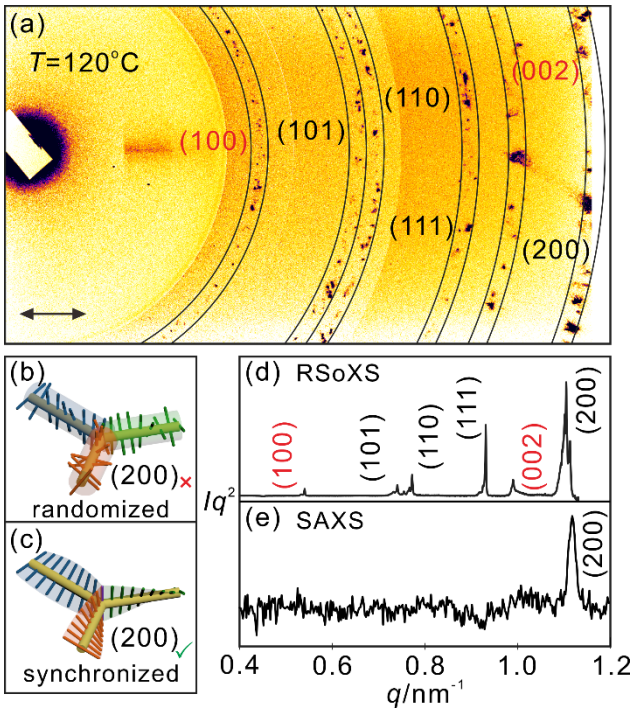

Fig. 5 (a) 2D RSoXS pattern of compound **1-18** near carbon K-edge (283.5 eV) at 120 °C upon heating. Six resonant signals can be indexed as a Tet_{bi} phase with two as 'forbidden peaks' in red. Black arrow indicates the direction of linear polarized X-ray. The horizontal shadow near beam stop, which is irrelevant with temperature, is a reflection from the substrate. Two distinct molecular packing models with (b) randomized and (c) synchronized twist along the networks. Only synchronized twist could generate the (200) resonant enhanced signal. (d) 1D diffractogram of (a), two 'forbidden peaks' (100) and (002) as well as a series of resonant enhanced peaks can be observed. (e) SAXS diffractogram in lower-q range of the Tet_{bi} phase at 120 °C. Only the (200) peak can be observed. The baseline fluctuations are severely due to the extremely low intensity of (200).

'Forbidden peaks', as a result of combining molecular orientations and particular space group, offer additional structural information as a complementary of SAXS. The coexistence of two 'forbidden peaks' (100) and (002) further supports our space group determination as the enantiomorphic space groups $P4_12_12/P4_32_12$ are the only pair of

tetragonal space groups allowing these two 'forbidden peaks' simultaneously.[70] Then, on the basis of the indexations from resonant signals, model-dependent resonant scattering simulations were carried out to illustrate the signal-structure relationship. Similar to our previous work on the $Ia\bar{3}d$ phase[52], by using the concept of 'resonant atom' and 'polarizability axis', we first considered two situations: one is the molecular strata form randomized twist, leading to a mismatch at the three-way junctions; another is the widely accepted continuous model with synchronized twist. The first one is actually composed of chirality randomized networks (Fig. 5b), which can be modeled by three resonant atoms at the junction with the polarizability axis direction pointing to three different directions along the segments. In contrast, the second is more complex, each stratum should be regarded as one resonant atom with polarizability axis pointing to specific directions to coincide with each other at the junction (Fig. 5c), see details of model construction in Section 6 of the SI. The Fourier transform of the models would give us a primary concept on resonant scattering signal. For the two models presented in Fig. 5b and 5c, randomized twist would not exhibit the (200) resonant enhanced signal. On contrary, (200) is allowed for synchronized twist as shown in Fig. 5c, see simulated results in Table S9. Thus, RSoXS suggests the Tet_{bi} phase contains synchronized twist in along at least one network. Additionally, the polarization of incident and scattered X-ray was taken into consideration to evaluate the scattering intensity and polarization of the 'forbidden peaks' (100) and (002), see Table S10.

3. Discussion

3.1 Partial network racemization breaks mirror symmetry

While RSoXS confirms synchronized twist in the Tet_{bi} phase, it can in principle be either uniform or opposite in adjacent networks. However, there can't be opposite twists along two networks with opposite chirality, which would cancel the chirality as in the $Ia\bar{3}d$ phase. Taking the space group chirality and network chirality into consideration, we raised an alternative molecular packing model for the Tet_{bi} phase. Transformed from the *meso*-structure of the $Ia\bar{3}d$ phase, the molecules along one network preserve their

uniform helical organization, whereas along every second network the helical twist correlation along the networks becomes short range and gradually their helicity is lost, which breaks the symmetry, as shown in Fig. 6.

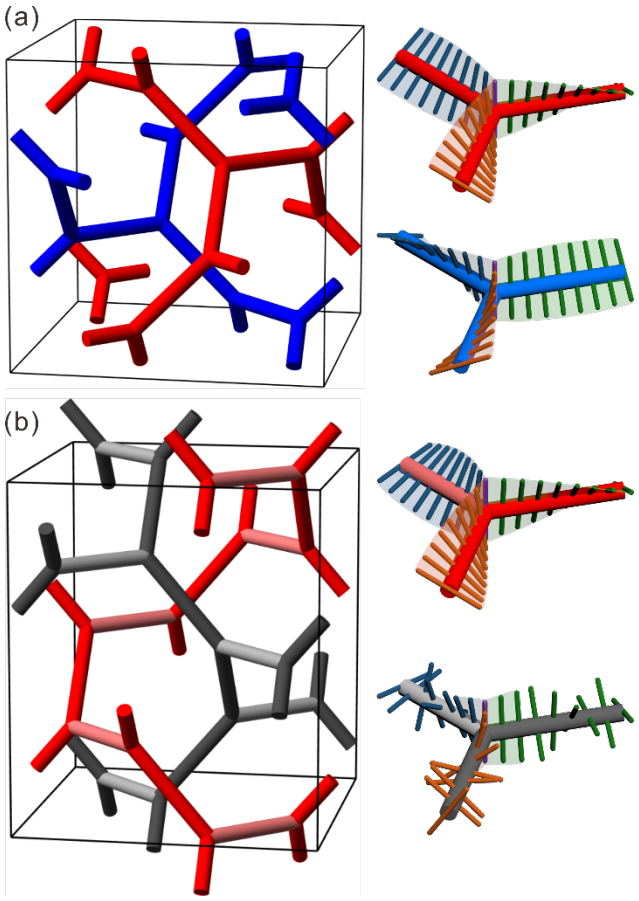

Fig. 6 (a) Schematic representation of $Ia\bar{3}d$ phase with red and blue networks showing opposite chirality. (b) $P4_12_12$ phase with one synchronized-twist network (red) and one randomized-twist network (gray). In the Tet_{bi} phase, the distorted networks consist of two longer segments (darker) and one shorter segment (lighter) at three-way junctions. The racemization of the twist in the gray network induces the formation of chirality in the Tet_{bi} phase.

Based on symmetry consideration, the 'forbidden peaks' of the Tet_{bi} phase contain (h00) when $h = 2n+1$ and (00l) when $l = 2n+1$ or $4n+2$ (Fig. 5d).[70] Those are in line with our simulated and experimental results including the 'forbidden peaks' (100) and (002), see details in Section 6 of the SI. Though alternative models with different twist angles in the two networks and those with identical twist sense in all helices would in principle also be in line with the SAXS and RSoXS data, these structures would lead to energetically unfavorable states which are due to a mismatch of the helical twist at the network

junctions. Therefore, these structures are unlikely as outlined in more detail in Figure S17 and the accompanying explanations in Section 8 of the SI.

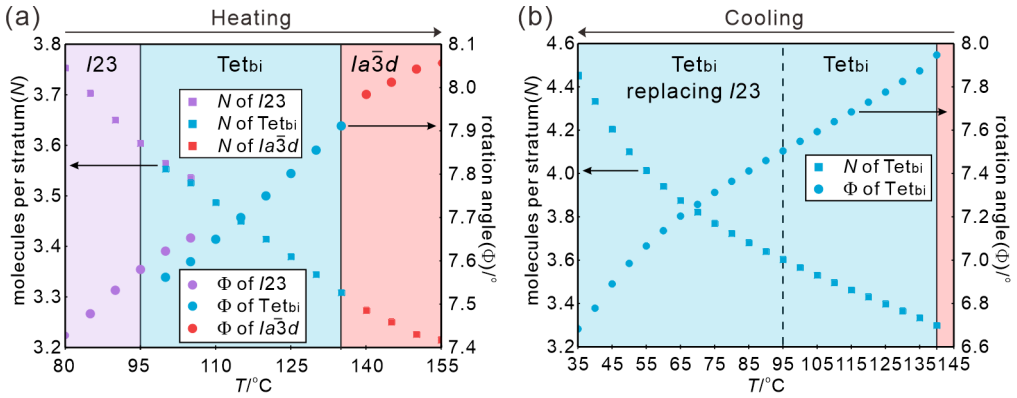

Fig. 7 The number of molecules per stratum (N, squares) and rotation angle Φ circles upon (a) heating and (b) cooling. The LC phases are represented by different colors: Purple is $I23$, blue is Tet_{bi} and red is $Ia\bar{3}d$. The dashed line in (b) indicates the $I23$-Tet_{bi} phase transition upon heating. The continuous variation and resemblance between $I23$ and Tet_{bi} phases support the phase transition sequence. With rising temperature, N decreases while Φ increases, which is a result of the thermal expansion of the aliphatic chains.

According to this model, we can derive a series of data based on lattice parameters and molecular organization, including number of molecules per stratum (N) and average rotation angle along the strata (Φ) for all three LC phases, see Fig. 7 and Tables S11-S12. Upon heating, N keeps decreasing, combined with an increasing Φ (decreasing helical pitch, see Fig. 7a) due to thermal chain expansion. Only in the Cub_{bi} phases (especially in $I23$) there is a marginally larger helical twist (Fig. 7a). The $I23$ phase once formed on heating is metastable and slowly (within 20-40 min) transforms into the more stable birefringent Tet_{bi} phase, which is then retained until crystallization takes place on cooling or to the transition to the $Ia\bar{3}d$ phase on heating. Hence, it appears that the Tet_{bi} phase allows a smaller twist Φ along the helical networks (Fig. 7b) than the competing $I23$ phase. As shown in Fig 7b, the slope of the $\Phi = f(T)$ curve increases below ~95 °C, indicating an even growing driving force for lattice expansion by reduction of Φ at lower temperature (see also Fig. S8c, d).

3.2 Transition between enantiophilic and enantiophobic network coupling

All these observations suggest that the Tet_{bi} phase is a stable intermediate phase at the transition between Cub_{bi} phases with $Ia\bar{3}d$ and *I*23 space group, as a result of the network transformation. It is postulated that this is mainly due to a change of the through-space interhelical interaction between adjacent networks. The $Ia\bar{3}d$ phase is composed of two enantiomorphic chiral networks (due to the 70.5° twist between the trigonal planes of the network junctions, see Fig. 6a). The combination of network chirality and helix sense leads to two energetically different (diastereomeric) states. As shown in Fig. 8a, the preferred energy minimum structure has opposite chirality of the networks and opposite helix sense of the supermolecular twist along these networks. Helices along two networks with opposite chirality exhibit exact opposite helical sense. This requires opposite helicity in adjacent networks, i.e. the mode of interhelix self-assembly is enantiophilic (heterochiral self-assembly), and the $Ia\bar{3}d$ phase thus represents an overall achiral *meso*-structure. However, this enantiophilic mode of self-assembly does not necessarily represent the preferred mode of the through-space helix-helix interaction, which is very sensitive to helical pitch, helix orientation and specific inter-helix interactions.[71-77] The $Ia\bar{3}d$ phase is stable as long as there is no helical superstructure, or the preferred helix-helix interaction remains more or less enantiophilic. As the *c*-parameter expands with decreasing temperature, some helix segments become longer and others shorter which modifies the helix-helix interactions (Fig. 8b). If the inter-helix interaction becomes enantiophobic, *i.e.*, the side-by-side packing of networks with identical helix sense becomes the preferred one (homochiral self-assembly), then a competition between the intrinsic enantiophilic network packing and the emerging enantiophobic helix-helix interaction arises. If the enantiophobic contribution of through-space helix-helix interactions becomes dominating (for **1-18** with lowering temperature) the chirality synchronization in one of the networks is given up, leading to ambidextrous mirror symmetry breaking with formation of a conglomerate of $P4_12_12$ and $P4_32_12$ domains. Racemization of one helix leads to $P4_12_12$, whereas racemization of the other one gives

$P4_32_12$. The size of the uniformly chiral domains of the conglomerate was estimated on the basis of the width of the peaks in the chirality sensitive RSoXS experiments. The full width at half maximum (FWHM) of the (200) peak is estimated to be < 0.02 nm^{-1}, so that the estimated size of the enantiomorphic $P4_12_12$ and $P4_32_12$ domains is at least in the range of 300-500 nm, corresponding to about 700-2000 times the area of a_{tet}^2, see Table S13 for details. Thus, a key feature is that the $Ia\bar{3}d$-to-Tet_{bi} transition takes place by racemization of every second network of the supramolecular *meso*-structure with $Ia\bar{3}d$ space group, leading to desymmetrization of the phase and emergence of chirality.

The hypothesized combination of different modes of self-assembly (helical + randomized) in a uniform phase structure is unusual, but not impossible if required by an emerging frustration force. For example, geometric frustration occurring at the transition from hard to soft spheres is known to force the combination of different spheres in the complex Frank Kasper type soft matter phases, including quasicrystalline.[78-79] Similarly, froth structures and clathrates combine different types of polyhedra to minimize interfacial area while retaining a periodic packing.[80] In the case reported here, the double gyroid is the most stable network structure intrinsically requiring enantiophilic helix-helix interactions, if formed by two helical networks. On the other hand, any emerging enantiophobic helix-helix interaction is incompatible with the double gyroid structure and thus requires either helix-randomization (leading to a helix free gyroid as known for flexible amphiphiles[28-30,52]) or a removal of the gyroid structure. However, the random packing of the transiently chiral molecules **1-18** (with twisted conformations[24,26]) in the networks is disfavored with respect to the denser helical organization, especially at lower temperature. In this competing situation, retaining only one helical network allows retention of a gyroid-like structure, while avoiding enantiophilic helix-helix interactions. However, at a certain strength of the enantiophobic interhelical interaction it becomes dominating and the lattice type is forced to change to an alternative phase structure, which is the Cub_{bi} phase with $I23$ lattice (Fig. 8c), being composed of three networks with identical helix sense (Fig. 1b).[25,47] In the case reported herein the driving force of enantiophobic interhelical through-space interaction appears to be not sufficiently strong

to permanently remove the double-gyroid-like structure and lead to a stable *I*23 phase, and in this case the Tet_{bi} phase with a stretched double gyroid becomes the stable mode of LC self-assembly.

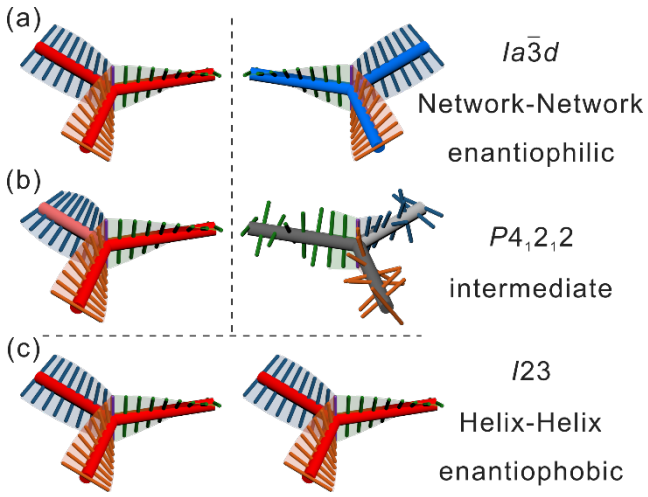

Fig. 8 Schematic representations of three-way junctions and molecular packing in (a) $Ia\bar{3}d$ phase, (b) $P4_12_12$ phase and (c) *I*23 phase, induced by the competition between enantiophobic/enantiophilic self-assembly. The domination of enantiophobic helix-helix interaction results in the ambidextrous chiral *I*23 phase. On the other hand, enantiophilic network-network interaction favors enantiomorphous networks in $Ia\bar{3}d$. Being an intermediate phase, the Tet_{bi} phase contains one racemic network while the other preserves helicity.

4. Conclusions

To conclude, we have comprehensively studied a new bicontinuous LC phase with tetragonal $P4_12_12/P4_32_12$ space group (Tet_{bi}) formed by polycatenar molecules, representing an intermediate LC phase between the chiral *I*23 and the achiral $Ia\bar{3}d$ Cub_{bi} phases. We raised a local molecular packing model verified by combination of RSoXS, SAXS, and model-dependent scattering simulations. Accordingly, the racemization of half of the networks breaks the symmetry and generates ambidextrous chirality during the transition from the supramolecular *meso*-structure of the $Ia\bar{3}d$ phase to the chiral Tet_{bi} phase. This provides a new mode of mirror symmetry breaking in soft self-assembled systems. This process is considered as a liquid state analogue to recently developed spontaneous deracemization techniques by crystallization of achiral or rapidly racemizing chiral molecules of solid crystalline materials[81-83], and could be used to produce chiral

soft materials from achiral molecules for use in various applications, for example, circular polarized emission and as soft chiral templates after fixation of a uniform macroscale chirality by further spontaneous (stochastic) or induced (directed) asymmetry amplification.[49-50,84]

5. Experimental Section

The synthesis and analytical data of compound **1-18** have been reported in ref. 37.

DSCs were recorded with a Perkin Elmer DSC-7 at a rate of 10 K min and optical investigations were conducted using a Leica DMRP-XP polarizing microscope in conjunction with a Mettler FP-82 HT hot stage.

Synchrotron small-angle X-ray scattering experiments were conducted at beamline 7.3.3 at Advanced Light Source (ALS) and beamline BL16B1 at Shanghai Synchrotron Radiation Facility (SSRF) with transmission mode. Samples were held in evacuated 1mm diameter capillaries. The exposure time used was 10-120 s. See SI for detailed facility parameters, calibration method and data processing software.

Resonant Soft X-ray Scattering (RSoXS) was recorded on BL11.1.0.2, Advanced Light Source, ALS with transmission mode. Sample film was prepared by a drop-casting between two pieces of silicon nitride glass. The exposure time used was 30-120s.

Full details of the used experimental methods and conditions are collated in the electronic supporting information.

ASSOCIATED CONTENT

Supporting Information

The Supporting Information is available free of charge at http://pubs.acs.org.

Experimental methods; additional experimental data; analysis of X-ray data, reconstruction of electron density maps and resonant/conventional X-ray scattering simulation from models; supporting discussion and calculations; SAXS profile and the RSoXS energy scan.

AUTHOR INFORMATION

Corresponding Authors

Feng Liu - Shaanxi International Research Center for Soft Matter, State Key Laboratory for Mechanical Behaviour of Materials, Xi'an Jiaotong University, Xi'an 710049, P. R. China; orcid.org/0000-0001-6224-5167. Email: feng.liu@xjtu.edu.cn

Carsten Tschierske − Institute of Chemistry, Martin-Luther-University Halle-Wittenberg, 06120 Halle, Germany; orcid.org/0000-0002-4163-3272; Email: carsten.tschierske@chemie.uni-halle.de

Authors

Yu Cao - Shaanxi International Research Center for Soft Matter, State Key Laboratory for Mechanical Behaviour of Materials, Xi'an Jiaotong University, Xi'an 710049, P. R. China; MOE Key Laboratory for Nonequilibrium Synthesis and Modulation of Condensed Matter, School of Physics, Xi'an Jiaotong University, Xi'an 710049, P. R. China. orcid.org/0000-0002-9134-8680.

Mohamed Alaasar − Institute of Chemistry, Martin-Luther-University Halle-Wittenberg, 06120 Halle, Germany; Department of Chemistry, Cairo University, 12613 Giza, Egypt. orcid.org/0000-0003-4155-8644.

Lei Zhang - MOE Key Laboratory for Nonequilibrium Synthesis and Modulation of Condensed Matter, School of Physics, Xi'an Jiaotong University, Xi'an 710049, P. R. China. orcid.org/0000-0002-4880-824X.

Chenhui Zhu - Advanced Light Source, Lawrence Berkeley National Laboratory, Berkeley, CA 94720, USA. orcid.org/0000-0003-1263-5065.

Complete contact information is available at: http://pubs.acs.org.

Notes

The authors declare no competing financial interest.

ACKNOWLEDGMENT

The authors acknowledge financial supporting from National Natural Science Foundation of China (21774099, 21761132033 and 11922410), Science and Technology Agency of Shaanxi Province (2016KW-050 and 2018KWZ-03) and the German Research Foundation (DFG, 24355983 and 436494874 - RTG 2670). The authors are grateful to Beamline BL16B1 at SSRF (Shanghai Synchrotron Radiation Facility, China) for providing the beamtime. Y.C. thanks China Scholarship Council (CSC) for providing financial support (201706280170). We acknowledge use of Beamlines 11.0.1.2 of the Advanced Light Source supported by the Director of the Office of Science, Office of Basic Energy Sciences, of the U.S. Department of Energy under contract no. DE-AC02-05CH11231.

REFERENCES:

(1) Lehn, J. M. Perspectives in supramolecular chemistry-from molecular recognition towards molecular information processing and self-organization. *Angew. Chem. Int. Ed.* **1990**, *29* (11), 1304-1319.

(2) Zhang, R.; Su, Z.; Yan, X. Y.; Huang, J.; Shan, W.; Dong, X. H.; Feng, X.; Lin, Z.; Cheng, S. Z. D. Discovery of Structural Complexity through Self-Assembly of Molecules Containing Rodlike Components. *Chem. Eur. J.* **2020**, *26* (30), 6741-6756.

(3) Liu, Y.; Liu, T.; Yan, X. X.; Guo, Q. Y.; Wang, J.; Zhang, R.; Zhang, S.; Su, Z.; Huang, J.; Liu, G. X.; Zhang, W.; Zhang, W.; Aida, T.; Yue, K.; Huang, M.; Cheng, S. Z. D. Mesoatom alloys via self-sorting approach of giant molecules blends. *Giant*, **2020**, *4*, 100031.

(4) Tschierske, C. Development of structural complexity by liquid crystal self-assembly, *Angew. Chem. Int. Ed.* **2013**, *52* (34), 8828-8878.

(5) Buhse, T.; Cruz, J. M.; Noble-Teran, M. E.; Hochberg, D.; Ribó, J. M.; Crusats, J.; Micheau, J. C. Spontaneous Deracemizations. *Chem. Rev.* **2021**, *121* (4), 2147-2229.

(6) Liu, M.; Zhang, L.; Wang, T. Supramolecular Chirality in Self-Assembled Systems. *Chem. Rev.* **2015**, *115* (15), 7304-7397.

(7) Shimizu, T.; Masuda, M.; Minamikawa, H. Supramolecular Nanotube Architectures

Based on Amphiphilic Molecules. *Chem. Rev.* **2005**, *105* (4), 1401-1443.

(8) Yashima, E.; Ousaka, N.; Taura, D.; Shimomura, K.; Ikai, T.; Maeda, K. Supramolecular Helical Systems: Helical Assemblies of Small Molecules, Foldamers, and Polymers with Chiral Amplification and Their Functions. *Chem. Rev.* **2016**, *116* (22), 13752-13990.

(9) Rao, K. V.; Miyajima, D.; Nihonyanagi, A.; Aida, T. Thermally bisignate supramolecular polymerization. *Nat. Chem.* **2017**, *9* (11), 1133-1139.

(10) Hill, J. P.; Jin, W.; Kosaka, A.; Fukushima, T.; Ichihara, H.; Shimomura, T.; Ito, K.; Hashizume, T.; Ishii, N.; Aida, T. Self-Assembled Hexa-peri-hexabenzocoronene Graphitic Nanotube. *Science*, **2004**, *304* (5676), 1481-1483.

(11) Hecht, M.; Leowanawat, P.; Gerlach, T.; Stepanenko, V.; Stolte, M.; Lehmann, M.; Würthner, F. Self-Sorting Supramolecular Polymerization: Helical and Lamellar Aggregates of Tetra-Bay-Acyloxy Perylene Bisimide. *Angew. Chem. Int. Ed.* **2020**, *59* (39), 17084-17090.

(12) Green, M. M.; Park, J. W.; Sato, T.; Teramoto, A.; Lifson, S.; Selinger, R. L. B.; Selinger, J. V. The Macromolecular Route to Chiral Amplification. *Angew. Chem., Int. Ed.* **1999**, *38* (21), 3138-3154.

(13) Borshch, V.; Kim, Y. K.; Xiang, J.; Gao, M.; Jakli, A.; Panov, V. P.; Vij, J. K.; Imrie, C. T.; Tamba, M. G.; Mehl, G. H.; Lavrentovich, O. D. Nematic twist-bend phase with nanoscale modulation of molecular orientation. *Nat. Commun.* **2013**, *4*, 2635.

(14) Wang, H. F.; Chiu, P. T.; Yang, C. Y.; Xie, Z. H.; Hung, Y. C.; Lee, J. Y.; Tsai, J. C.; Prasad, I.; Jinnai, H.; Thomas, E. L.; Ho, R. M. Networks with controlled chirality via self-assembly of chiral triblock terpolymers. *Sci. Adv.* **2020**, *6* (42), eabc3644.

(15) Palmans, A. R. A.; Meijer, E. W.; Denmark, S. E. Stereochemical language in supramolecular polymer chemistry: how we can do better. *J. Polym Sci.* **2021**, *59* (12), 1171-1174.

(16) Palmans, A. R. A.; Meijer, E. W. Amplification of chirality in dynamic supramolecular aggregates. *Angew. Chem. Int. Ed.* **2007**, *46* (47), 8948-8968.

(17) Dorca, Y; Greciano, E. E.; Valera, J. S.; Gjmez, R.; Sanchez, L. Hierarchy of

asymmetry in chiral supramolecular polymers: toward functional, helical supramolecular structures. *Chem. Eur. J.* **2019**, *25* (23), 5848-5864.

(18) Stals, P. J. M.; Korevaar, P. A.; Gillissen, M. A. J.; de Greef, T. F. A.; Fitie, C. F. C., Sijbesma, R. P.; Palmans, A. R. A.; Meijer; E. W. Symmetry breaking in the self-assembly of partially fluorinated benzene-1,3,5-tricarboxamides. *Angew. Chem. Int. Ed.* **2012**, *51* (45), 11297-11301.

(19) Li, Y.; Hammoud, A.; Bouteiller, L.; Raynal, M. Emergence of Homochiral Benzene-1,3,5-tricarboxamide Helical Assemblies and Catalysts upon Addition of an Achiral Monomer. *J. Am. Chem. Soc.* **2020**, *142* (12), 5676-5688.

(20) Shu, J.; Dudenko, D.; Esmaeili, M.; Park, J. H.; Puniredd, S. R.; Chang, J. Y.; Breiby, D. W.; Pisula, W. Hansen, M. R. Coexistence of Helical Morphologies in Columnar Stacks of Star-Shaped Discotic Hydrazones. *J. Am. Chem. Soc.* **2013**, *135* (30), 11075-11086

(21) Roche, C.; Sun, H. J.; Prendergast, M. E.; Leowanawat, P.; Partridge, B. E.; Heiney, P. A.; Araoka, F.; Graf, R.; Spiess, H. W.; Zeng, X.; Ungar, G.; Percec, V. Homochiral Columns Constructed by Chiral Self-Sorting During Supramolecular Helical Organization of Hat-Shaped Molecules. *J. Am. Chem. Soc.* **2014**, *136* (19), 7169-7185;

(22) Percec, V.; Xiao, Q. Helical chirality in supramolecular Columns and spheres Self-organized liquid crystals, and quasicrystals, *Isr. J. Chem*. **2021**, *61* (9-10), 530-556.

(23) Tschierske C. Mirror symmetry breaking in liquids and liquid crystals. *Liq. Cryst.* **2018**, *45* (13-15), 2221-2252.

(24) Tschierske, C.; Ungar, G. Mirror symmetry breaking by chirality synchronization in liquids and liquid crystals of achiral molecules. *ChemPhysChem* **2016**, *17* (1), 9-26.

(25) Dressel, C.; Liu, F.; Prehm, M.; Zeng, X.; Ungar, G.; Tschierske, C. Dynamic mirror‐symmetry breaking in bicontinuous cubic phases. *Angew. Chem. Int. Ed.* **2014**, *53* (48), 13115-13120.

(26) Dressel, C.; Reppe, T.; Prehm, M.; Brautzsch, M.; Tschierske, C. Chiral self-sorting and amplification in isotropic liquids of achiral molecules. *Nat. Chem.* **2014**, *6* (11),

971-977.

(27) Luzzati, V.; Tardieu, A.; Gulik-Krzywicki, T.; Rivas, E.; Reiss-Husson, F. Structure of the cubic phases of lipid–water systems. *Nature* **1968**, *220* (5166), 485-488.

(28) Hyde, S.; Blum, Z.; Landh, T.; Lidin, S.; Ninham, B.; Andersson, S.; Larsson, K. *The language of shape: the role of curvature in condensed matter: physics, chemistry and biology*; Elsevier, 1996.

(29) Lynch, M. L.; Spicer, P. T. *Bicontinuous liquid crystals*; CRC press, 2005.

(30) Meuler, A. J.; Hillmyer, M. A.; Bates, F. S. Ordered network mesostructures in block polymer materials. *Macromolecules* **2009**, *42* (19), 7221-7250.

(31) Saranathan, V.; Osuji, C. O.; Mochrie, S. G.; Noh, H.; Narayanan, S.; Sandy, A.; Dufresne, E. R.; Prum, R. O. Structure, function, and self-assembly of single network gyroid (I4132) photonic crystals in butterfly wing scales. *P. Natl. Acad. Sci. USA.* **2010**, *107* (26), 11676-11681.

(32) Han, L.; Che, S. An overview of materials with triply periodic minimal surfaces and related geometry: from biological structures to self-assembled systems. *Adv. Mater.* **2018**, *30* (17), 1705708.

(33) Kato, T.; Uchida, J.; Ichikawa, T.; Sakamoto, T. Functional liquid crystals towards the next generation of materials. *Angew. Chem. Int. Ed.* **2018**, *57* (16), 4355-4371.

(34) Zeng, X.; Poppe, S.; Lehmann, A.; Prehm, M.; Chen, C.; Liu, F.; Lu, H.; Ungar, G.; Tschierske, C. A Self-Assembled Bicontinuous Cubic Phase with a Single-Diamond Network. *Angew. Chem. Int. Ed.* **2019**, *58* (22), 7375-7379.

(35) Chen, C.; Kieffer, R.; Ebert, H.; Prehm, M.; Zhang, R. b.; Zeng, X.; Liu, F.; Ungar, G.; Tschierske, C. Chirality Induction through Nano-Phase Separation: Alternating Network Gyroid Phase by Thermotropic Self - Assembly of X - Shaped Bolapolyphiles. *Angew. Chem. Int. Ed.* **2020**, *59* (7), 2725-2729.

(36) Poppe, S.; Cheng, X.; Chen, C.; Zeng, X.; Zhang, R.-b.; Liu, F.; Ungar, G.; Tschierske, C. Liquid Organic Frameworks: The Single-Network "Plumber's Nightmare" Bicontinuous Cubic Liquid Crystal. *J. Am. Chem. Soc.* **2020**, *142* (7),

3296-3300.

(37) Morey, M.; Davidson, A.; Stucky, G. Silica-based, cubic mesostructures: Synthesis, characterization and relevance for catalysis. *J. Porous. Mat.* **1998**, *5* (3), 195-204.

(38) Vallet-Regi, M.; Rámila, A.; Del Real, R.; Pérez-Pariente, J. A new property of MCM-41: drug delivery system. *Chem. Mater.* **2001**, *13* (2), 308-311.

(39) Crossland, E. W.; Kamperman, M.; Nedelcu, M.; Ducati, C.; Wiesner, U.; Smilgies, D. M.; Toombes, G. E. S.; Hillmyer, M. A.; Ludwigs, S.; Steiner, U.; et al. A Bicontinuous Double Gyroid Hybrid Solar Cell. *Nano. Lett.* **2009**, *9* (8), 2807-2812.

(40) Ichikawa, T.; Yoshio, M.; Hamasaki, A.; Taguchi, S.; Liu, F.; Zeng, X.; Ungar, G.; Ohno, H.; Kato, T. Induction of thermotropic bicontinuous cubic phases in liquid-crystalline ammonium and phosphonium salts. *J. Am. Chem. Soc.* **2012**, *134* (5), 2634-2643.

(41) Kwon, O.; Cai, X.; Qu, W.; Liu, F.; Szydłowska, J.; Gorecka, E.; Han, M. J.; Yoon, D. K.; Poppe, S.; Tschierske, C. Charge Transportation and Chirality in Liquid Crystalline Helical Network Phases of Achiral BTBT - Derived Polycatenar Molecules. *Adv. Funct. Mater.* **2021**, 2102271.

(42) Kutsumizu, S. Recent progress in the synthesis and structural clarification of thermotropic cubic phases. *Isr. J. Chem.* **2012**, *52* (10), 844-853.

(43) Ozawa, K.; Yamamura, Y.; Yasuzuka, S.; Mori, H.; Kutsumizu, S.; Saito, K. Coexistence of Two Aggregation Modes in Exotic Liquid-Crystalline Superstructure: Systematic Maximum Entropy Analysis for Cubic Mesogen, 1, 2-Bis (4′-n-alkoxybenzoyl) hydrazine [BABH (n)]. *J. Phys. Chem. B.* **2008**, *112* (39), 12179-12181.

(44) Vaupotič, N.; Salamończyk, M.; Matraszek, J.; Vogrin, M.; Pociecha, D.; Gorecka, E. New structural model of a chiral cubic liquid crystalline phase. *Phys. Chem. Chem. Phys.* **2020**, *22* (22), 12814-12820.

(45) Levelut, A.-M.; Clerc, M. Structural investigations on 'smectic D' and related mesophases. *Liq. Cryst.* **1998**, *24* (1), 105-116.

(46) Zeng, X.; Ungar, G.; Impéror-Clerc, M. A triple-network tricontinuous cubicliquid

crystal. *Nat. Mater.* **2005**, *4* (7), 562-567.

(47) Zeng, X.; Ungar, G. Spontaneously chiral cubic liquid crystal: three interpenetrating networks with a twist. *J. Mater. Chem. C* **2020**, *8* (16), 5389-5398.

(48) Kutsumizu, S.; Misako, S.; Miwa, Y.; Kitagawa M.; Yamamura, Y.; Saito, K. Mirror symmetry breaking by mixing of equimolar amounts of two gyroid phase-forming achiral molecules. *Phys. Chem. Chem. Phys.* **2016**, *18* (26), 17341-17344.

(49) Tschierske, C.; Dressel, C. Mirror Symmetry Breaking in Liquids and Their Impact on the Development of Homochirality in Abiogenesis: Emerging Proto-RNA as Source of Biochirality? *Symmetry* **2020**, *12* (7), 1098.

(50) Sang, Y.; Yang, D.; Shen, Z.; Duan, P.; Liu, M. Mechanically Controlled and Consecutively Boosted Circularly Polarized Luminescence of Nanoassemblies from Achiral Molecules. *J. Phys. Chem. C* **2020**, *124* (31), 17274-17281

(51) Green, M. M.; Jain, V. Homochirality in life: Two equal runners, one tripped. *Origins. Life. Evol. B.* **2010**, *40* (1), 111-118.

(52) Cao, Y.; Alaasar, M.; Nallapaneni, A.; Salamończyk, M.; Marinko, P.; Gorecka, E.; Tschierske, C.; Liu, F.; Vaupotič, N.; Zhu, C. Molecular packing in double gyroid cubic phases revealed via resonant soft X-Ray scattering. *Phy. Rev. Lett.* **2020**, *125* (2), 027801.

(53) Kutsumizu, S.; Yamada, M.; Yano, S. Mesomorphic phase transitions of a series of D-phase compounds. *Liq. Cryst.* **1994**, *16* (6), 1109-1113.

(54) Goodby, J.; Dunmur, D.; Collings, P. J. Lattice melting at the clearing point in frustrated systems. *Liq. Cryst.* **1995**, *19* (5), 703-709.

(55) Reppe, T.; Poppe, S.; Cai, X.; Cao, Y.; Liu, F.; Tschierske, C. Spontaneous mirror symmetry breaking in benzil-based soft crystalline, cubic liquid crystalline and isotropic liquid phases. *Chem. Sci.* **2020**, *11* (23), 5902-5908.

(56) Müller, U. *Symmetry relationships between crystal structures: applications of crystallographic group theory in crystal chemistry*; OUP Oxford, 2013.

(57) Lu, H.; Zeng, X.; Ungar, G.; Dressel, C.; Tschierske, C. The solution of the puzzle of smectic-Q: the phase structure and the origin of spontaneous chirality. *Angew.*

Chem. Int. Ed. **2018**, *57* (11), 2835-2840.

(58) Cao, Y.; Feng, C.; Jakli, A.; Zhu, C.; Liu, F. Deciphering chiral structures in soft materials via resonant soft and tender X-ray scattering. *Giant* **2020**, 100018.

(59) Zhu, C.; Wang, C.; Young, A.; Liu, F.; Gunkel, I.; Chen, D.; Walba, D.; Maclennan, J.; Clark, N.; Hexemer, A. Probing and controlling liquid crystal helical nanofilaments. *Nano. Lett.* **2015**, *15* (5), 3420-3424.

(60) Zhu, C.; Tuchband, M. R.; Young, A.; Shuai, M.; Scarbrough, A.; Walba, D. M.; Maclennan, J. E.; Wang, C.; Hexemer, A.; Clark, N. A. Resonant carbon K-edge soft X-ray scattering from lattice-free heliconical molecular ordering: soft dilative elasticity of the twist-bend liquid crystal phase. *Phys. Rev. Lett.* **2016**, *116* (14), 147803.

(61) Salamończyk, M.; Vaupotič, N.; Pociecha, D.; Wang, C.; Zhu, C.; Gorecka, E. Structure of nanoscale-pitch helical phases: blue phase and twist-bend nematic phase resolved by resonant soft X-ray scattering. *Soft Matter* **2017**, *13* (38), 6694-6699.

(62) Stevenson, W.; Ahmed, Z.; Zeng, X.; Welch, C.; Ungar, G.; Mehl, G. Molecular organization in the twist–bend nematic phase by resonant X-ray scattering at the Se K-edge and by SAXS, WAXS and GIXRD. *Phys. Chem. Chem. Phys.* **2017**, *19* (21), 13449-13454.

(63) Salamończyk, M.; Mandle, R. J.; Makal, A.; Liebman-Peláez, A.; Feng, J.; Goodby, J. W.; Zhu, C. Double helical structure of the twist-bend nematic phase investigated by resonant X-ray scattering at the carbon and sulfur K-edges. *Soft Matter* **2018**, *14* (48), 9760-9763.

(64) Green, A. A. S.; Tuchband, M. R.; Shao, R.; Shen, Y.; Visvanathan, R.; Duncan, A. E.; Lehmann, A.; Tschierske, C.; Carlson, E. D.; Guzman, E.; et al. Chiral Incommensurate Helical Phase in a Smectic of Achiral Bent-Core Mesogens. *Phys. Rev. Lett.* **2019**, *122* (10), 107801.

(65) Salamończyk, M.; Vaupotič, N.; Pociecha, D.; Walker, R.; Storey, J. M.; Imrie, C. T.; Wang, C.; Zhu, C.; Gorecka, E. Multi-level chirality in liquid crystals formed by achiral molecules. *Nat. Commun.* **2019**, *10* (1), 1-8.

(66) Tuchband, M. R.; Paterson, D. A.; Salamończyk, M.; Norman, V. A.; Scarbrough, A. N.; Forsyth, E.; Garcia, E.; Wang, C.; Storey, J. M. D.; Walba, D. M.; et al. Distinct differences in the nanoscale behaviors of the twist–bend liquid crystal phase of a flexible linear trimer and homologous dimer. *P. Natl. Acad. Sci. USA.* **2019**, *116* (22), 10698.

(67) Feng, C.; Feng, J.; Saha, R.; Arakawa, Y.; Gleeson, J.; Sprunt, S.; Zhu, C.; Jákli, A. Manipulation of the nanoscale heliconical structure of a twist-bend nematic material with polarized light. *Phys. Rev. Res.* **2020**, *2* (3), 032004.

(68) Cao, Y.; Feng, J.; Nallapaneni, A.; Arakawa, Y.; Zhao, K.; Zhang, H.; Mehl, G. H.; Zhu, C.; Liu, F. Deciphering helix assembly in the heliconical nematic phase via tender resonant X-ray scattering. *J. Mater. Chem. C* **2021**, *9* (31), 10020-10028.

(69) Zhong, W. K.; Liu, F.; Wang, C. Probing morphology and chemistry in complex soft materials with in situ resonant soft x-ray scattering. *J. Phys.: Condens. Matter,* **2021**, *33* (31), 313001.

(70) Morgenroth, W.; Kirfel, A.; Fischer, K. Anisotropy of anomalous scattering in X-ray diffraction.'Forbidden'axial reflections in tetragonal space groups. *Z. Krist-Cryst. Mater.* **1994**, *209* (2), 124-131.

(71) Harris, A. B.; Kamien, R. D.; Lubensky, T. C. Molecular chirality and chiral parameters. *Rev. Mod. Phys.* **1999**, *71* (5), 1745.

(72) Lin, J.; Guo, Z.; Plas, J.; Amabilino, D. B.; De Feyter, S.; Schenning, A. P. Homochiral and heterochiral assembly preferences at different length scales–conglomerates and racemates in the same assemblies. *Chem. Commun.* **2013**, *49* (81), 9320-9322.

(73) Xu, F.; Khan, I. J.; McGuinness, K.; Parmar, A. S.; Silva, T.; Murthy, N. S.; Nanda, V. Self-assembly of left-and right-handed molecular screws. *J. Am. Chem. Soc.* **2013**, *135* (50), 18762-18765.

(74) Diaz-Cabrera, S.; Dorca, Y.; Calbo, J.; Arago, J.; Gomez, R.; Orti, E.; Sanchez, L. Hierarchy of Asymmetry at Work: Chain-Dependent Helix-to-Helix Interactions in Supramolecular Polymers. *Chem. Eur. J.* **2018**, *24* (12), 2826-2831.

(75) Efrati, E.; Irvine, W. T. M. Orientation-Dependent Handedness and Chiral Design. *Phys. Rev. X* **2014**, *4*, 011003.

(76) Grason, G. M. *Colloquium*: Geometry and optimal packing of twisted columns and filaments. *Rev. Mod. Phys.* **2015**, *87*, 401.

(77) Frezza, E.; Ferrarini, A.; Kolli, H. B.; Giacometti, A.; Cinacchi, G. Left or right cholesterics? A matter of helix handedness and curliness. *Phys. Chem. Chem. Phys.* **2014**, *16* (30), 16225-16232.

(78) Baez-Cotto, C. M.; Mahanthappa, M. K. Micellar mimicry of intermetallic C14 and C15 laves phases by aqueous lyotropic self-assembly. *ACS Nano* **2018**, *12* (4), 3226-3234.

(79) Su, Z.; Hsu, C.-H.; Gong, Z.; Feng, X.; Huang, J.; Zhang, R.; Wang, Y.; Mao, J.; Wesdemiotis, C.; Li, T.; et al. Identification of a Frank–Kasper Z phase from shape amphiphile self-assembly. *Nat. Chem*. **2019**, *11* (10), 899-905.

(80) Sadoc, J.-F.; Rivier, N. *Foams and emulsions*; Springer Science & Business Media, 2013.

(81) Matsuura, T.; Koshima, H. Introduction to chiral crystallization of achiral organic compounds: Spontaneous generation of chirality. *J. Photoch. Photobio. C* **2005**, *6* (1), 7-24.

(82) Amabilino, D. B.; Kellogg, R. M. Spontaneous deracemization. *Isr. J. Chem.* **2011**, *51* (10), 1034-1040.

(83) Sögütoglu, L. C.; Steendam, R. R.; Meekes, H.; Vlieg, E.; Rutjes, F. P. Viedma ripening: a reliable crystallisation method to reach single chirality. *Chem. Soc. Rev.* **2015**, *44* (19), 6723-6732.

(84) Zheng, Z. J.; Lu, Y. Q.; Li, Q. Photoprogrammable Mesogenic Soft Helical Architectures: A Promising Avenue toward Future Chiro-Optics. *Adv. Mater.* **2020**, *32* (41), 1905318

TOC

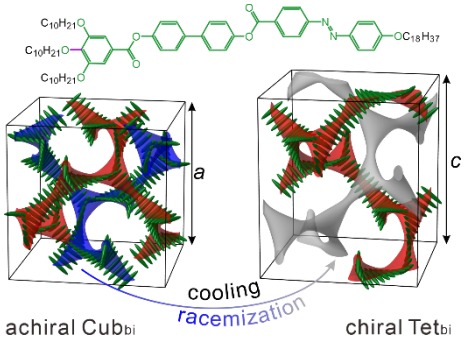
$C_{10}H_{21}O$
$C_{10}H_{21}O$
$C_{10}H_{21}O$
$OC_{18}H_{37}$
a
c
cooling
racemization
achiral Cub_{bi}
chiral Tet_{bi}